

Investigating Privacy Leakage in Dimensionality Reduction Methods via Reconstruction Attack

Chayadon Lumbut*

Donlapark Ponnoprat*[†]

Abstract

This study investigates privacy leakage in dimensionality reduction methods through a novel machine learning-based reconstruction attack. Employing an *informed adversary* threat model, we develop a neural network capable of reconstructing high-dimensional data from low-dimensional embeddings.

We evaluate six popular dimensionality reduction techniques: PCA, sparse random projection (SRP), multidimensional scaling (MDS), Isomap, *t*-SNE, and UMAP. Using both MNIST and NIH Chest X-ray datasets, we perform a qualitative analysis to identify key factors affecting reconstruction quality. Furthermore, we assess the effectiveness of an additive noise mechanism in mitigating these reconstruction attacks.

1 Introduction

Machine Learning (ML) models have become essential tools for solving complex real-world problems across various domains, including image processing, natural language processing, and business analytics. However, learning from high-dimensional data can be difficult due to the curse of dimensionality and increased computational requirements. To address these issues, dimensionality reduction methods are employed in order to reduce training costs and improve its efficiency.

Popular dimensionality reduction methods include principal component analysis, *t*-SNE [vdMH08], and UMAP [MHM18]. These methods aim to reduce data dimensions while preserving global and local properties of the original data, ensuring that relationships between data points in higher dimensions are still reflected in lower-dimensional representations. The information retained from the original data is crucial for effective data analysis and visualization.

However, the widespread use of dimensionality reduction methods on sensitive data has posed privacy risks, particularly in sensitive domains like face recognition [LX20], genomics [Pla13, KB19, CCR+20], and healthcare [TEAYT+19, DSK+23]. While low-dimensional representations enable efficient analysis and valuable insights, they also pose significant privacy threats. The core of this risk lies in the information preserved by dimensionality reduction methods, in particular, the relationships between data points. This preservation potentially allows adversaries to gain some information about the original high-dimensional data or determine whether a specific individual's data was included in the training set.

Among privacy attacks, two types are particularly noteworthy: membership inference attacks [SSSS17] aim to determine whether a specific data point was part of the training set of

*Chiang Mai University, Chiang Mai, Thailand.

[†]Corresponding author: donlapark.p@cmu.ac.th

the target ML model. By querying the model and analyzing its behavior for different inputs, attackers can exploit the vulnerabilities caused by overfitting to infer the membership status of individual data points. Even more severe are reconstruction attacks [CLE⁺19, CTW⁺21], which attempt to reconstruct the original data from the transformed or reduced-dimensional representations. These attacks typically assume the attacker has access to some data with the same distribution as the training set, knowledge of the model architecture, or statistical information about the population from which the training set is drawn.

Dimensionality reduction methods vary widely in their approaches, leading to differences in privacy leakage when their outputs are released. These differences stem from the varying degrees of randomization during training and the information preserved in the outputs. **This paper aims to compare privacy leakages from different dimensionality reduction methods using a reconstruction attack framework.** To achieve this, we propose a framework that includes a threat model and a reconstruction attack. Our framework is designed to be applicable across various dimensionality reduction methods. Additionally, we propose a defense strategy against the reconstruction attack, which, as a consequence, offers protection against weaker attacks.

A summary of our contribution Our work presents the following contribution:

- We propose a threat model and a reconstruction attack that can be applied to any dimensionality reduction method.
- Using this attack, we investigate and compare the privacy leakage from six popular dimensionality reduction methods. In our main study, we apply the attack on two specific datasets in order to identify underlying factors that affect the reconstruction quality.
- We investigate a simple additive noise mechanism and how much the noise’s scale affects the reconstruction quality of each dimensionality reduction method.

As a result, our study reveals which dimensionality reduction methods are more resilient to privacy attacks, and which better retain the information after applying the defense mechanism.

2 Background

2.1 Dimensionality reduction methods

Setting. Let $D = \{x_1, \dots, x_n\} \in (\mathbb{R}^d)^n = \mathbb{R}^{n \times d}$ be a dataset of n data points in \mathbb{R}^d . Given $d > 2$, a dimensionality reduction algorithm $M : \mathbb{R}^{n \times d} \rightarrow \mathbb{R}^{n \times 2}$ is a (possibly randomized) model that maps the d -dimensional dataset to 2-dimensional one: $\theta = M(D)$. Here, θ , referred to as a *low-dimensional embedding* of D , can be reshaped as a vector of $2n$ parameters of M fitted on D .

There are numerous dimensionality reduction methods. Among these, we shall focus on six methods that are often used on high-dimensional datasets [NBA⁺21, XZS⁺22]. We give a quick overview of each dimensionality reduction technique.

1. **Principal component analysis (PCA).** PCA [Pea01, Hot33] is one of the most popular and widely used dimensionality reduction methods. It is used to reduce high-dimensional data into lower-dimensional representations by projecting the data onto directions with the highest variations. These directions are obtained by decomposing the covariance matrix of the data

into eigenvectors and eigenvalues. The eigenvectors with the highest eigenvalues represent the directions of the greatest variances, known as the *principal components*. By projecting the original data onto these principal components, PCA achieves a lower-dimensional representation while preserving the variation in the dataset.

In particular, we reduce the data to two dimensions by projecting them to the first two principal components.

2. **Sparse random projection (SRP).** *Random projection* refers to a data reduction technique where each data point is projected onto a r -dimensional subspace ($r = 2$ in our case) via a random matrix R of size $d \times r$, whose elements are typically sampled from a normal distribution: Denoting our original data by $D_{n \times d}$ and the random projection matrix by $R_{d \times r}$, the data in low dimension $\theta_{n \times r}$ is given by:

$$\theta_{n \times r} = D_{n \times d} R_{d \times r}$$

A well-known lemma by [JL84] states that the projection approximately preserves the pairwise distances. Nonetheless, the complexity of the matrix multiplication is of order $O(n dr)$, which can be computationally expensive. To reduce the computation, sparse random projection [Ach01, LHC06] was proposed, in which the dense random matrix $R_{d \times r}$ is replaced by a sparse matrix $R_{d \times r}^{\text{sparse}}$, whose elements are:

$$R_{d \times r}^{\text{sparse}}[i, j] = \begin{cases} -\sqrt{\frac{d}{r}} & \text{with probability } \frac{1}{2d} \\ 0 & \text{with probability } 1 - \frac{1}{d} \\ \sqrt{\frac{d}{r}} & \text{with probability } \frac{1}{2d} \end{cases}.$$

As the average number of nonzero entries in each column of $R_{d \times r}^{\text{sparse}}$ is $d \cdot \frac{1}{d} = 1$, using this projection matrix results in a much faster computation of $O(nr)$ on average. [LHC06] show that the embedding quality of SRP is comparable to the classical random projection while being much more computationally efficient.

3. **Multidimensional scaling (MDS).** MDS finds a low-dimensional embedding $\theta = \{\theta_1, \dots, \theta_n\}$ of data $D = \{x_1, \dots, x_n\}$ through minimizing an objective known as the *stress function*:

$$\text{Stress}(\theta) = \sum_{1 \leq i < j \leq n} (\|\theta_i - \theta_j\| - \|x_i - x_j\|)^2. \quad (1)$$

In other words, the stress function measures the discrepancies between the pairwise distances in the original space and those in the embedded space. There are many ways to minimize the function. In particular, we use an iterative steepest descent approach proposed by [Kru64].

4. **Isometric Mapping (Isomap).**

Isomap [TSL00] was motivated by an observation that the Euclidean distance used in MDS fails to capture non-linear structure in high-dimensional data. For example, consider a simple data consisting of two points lying on opposite sides of a ball's surface. The Euclidean distance between these two points would not coincide with the surface distance from one point to the other. Isomap aims to embed data in a lower dimensional space while preserving the "surface distance" (referred to as *geodesic distance*) in the high-dimensional space. This is done by performing the following steps:

- (a) Establish a graph G with nodes x_1, \dots, x_n . For each x_i, x_j is connected to x_i if is one of the k nearest neighbors of x_i , and the edge is weighted by the distance $\|x_i - x_j\|$.
- (b) For all i, j , calculate the distance $d^G(x_i, x_j)$, given by the shortest path in G from x_i to x_j . Let A^G be the distance matrix whose (i, j) -th entry is $d^G(x_i, x_j)$.
- (c) Apply MDS on the pairwise shortest path $d^G(x_i, x_j)$. It can be shown that the r -dimensional embedding is given by [TSL00]:

$$\theta = \Lambda^{1/2}V^T,$$

where Λ is the diagonal matrix of the top- r eigenvalues and V is the top- r eigenvectors of $-\frac{1}{2}HA^GH^T$. Here, $H = I_n - \frac{1}{n}\mathbf{1}_n\mathbf{1}_n^T$ is the centering matrix (with $\mathbf{1}_n = (1, \dots, 1)^T$).

5. **t -stochastic neighbor embedding (t -SNE).** t -SNE [vdMH08] approaches dimensionality reduction as an optimization problem, similar to MDS. The method begins by modeling the pairwise relationships between the original high-dimensional data points using a Gaussian kernel:

$$p_{j|i} = \frac{e^{-\|x_i - x_j\|^2/2\sigma_i^2}}{\sum_{k \neq i} e^{-\|x_i - x_k\|^2/2\sigma_i^2}}, \quad \text{for } j \neq i, \quad p_{i|i} = 0.$$

The Gaussian bandwidth σ_i essentially determines that x_i should not be farther than two or three multiples of σ from x_i to be considered a neighbor of x_i , since with more than three multiples of σ_i , the numerator of $p_{i|j}$ becomes very small. See [vdMH08] for the recommended searching procedure for σ_i .

As $\sum_{i,j} p_{i|j} = n$, we define the symmetrized probability $p_{ij} = (p_{i|j} + p_{j|i})/2n$ which yields $\sum_{ij} p_{ij} = 1$. On the other hand, the pairwise distances between the embedded points $\theta = \{\theta_1, \dots, \theta_n\}$ are modeled through the Student's t kernel:

$$q_{ij} = \frac{(1 + \|\theta_i - \theta_j\|^2)^{-1}}{\sum_k \sum_{l \neq k} (1 + \|\theta_k - \theta_l\|^2)^{-1}}$$

With the discrete probability distributions $P = (p_{ij})_{1 \leq i, j \leq n}$ and $Q = (q_{ij})_{1 \leq i, j \leq n}$, the dissimilarities between the pairwise distances in the original and embedded spaces are measured through the Kullback-Leibler divergence between P and Q :

$$f_{t\text{-SNE}}(\theta) = \text{KL}(P||Q) = \sum_{i \neq j} p_{ij} \log \frac{p_{ij}}{q_{ij}}.$$

A low-dimensional embedding can be obtained by minimizing $f_{t\text{-SNE}}(\theta)$ with respect to θ . In the high-dimensional space, the Gaussian kernel used in p_{ij} helps maintain the local structure of the data. Conversely, in the low-dimensional space, the heavy-tailed Student's t kernel used in q_{ij} allows for greater separation between dissimilar points, thereby preserving meaningful global structure in the embedding.

6. **Uniform manifold approximation and projection (UMAP).** UMAP [MHM18] uses the same idea as t -SNE in that they model the pairwise distances in high-dimensional and low-dimensional spaces through discrete probabilities, with the following modifications: For each

$x_i \in D$, let ρ_i be the distance from x_i to its nearest neighbor. With a specified number of nearest neighbors k , we define

$$p_{i|j} = \begin{cases} e^{-(\|x_i - x_j\| - \rho_i)/\sigma_i} & j \in \{k \text{ nearest neighbors of } x_i\} \\ 0 & \text{otherwise.} \end{cases}$$

The symmetrized probability is defined as $p_{ij} = p_{i|j} + p_{j|i} - p_{i|j}p_{j|i}$. Note that $\sum_{ij} p_{ij}$ is not necessarily one. The pairwise distances in the low-dimensional space is modeled through:

$$q_{ij} = \frac{1}{1 + a\|\theta_i - \theta_j\|^{2b}},$$

which is similar to an unnormalized Student's t kernel. Data-driven procedures to find suitable choices of k , σ_i , a and b are fully explained in [MHM18].

Finally, with $P = (p_{ij})_{1 \leq i, j \leq n}$ and $Q = (q_{ij})_{1 \leq i, j \leq n}$, the optimization objective for UMAP is the cross-entropy loss:

$$f_{\text{UMAP}}(\theta) = \text{CE}(P, Q) = - \sum_{i \neq j} \{p_{ij} \log q_{ij} + (1 - p_{ij}) \log(1 - q_{ij})\}.$$

As with t -SNE, we minimize $f_{\text{UMAP}}(\theta)$ with respect to θ in order to find a suitable low-dimensional embedding of D .

One key observation that will be brought up again in the discussion of our experiments is that these methods can be divided into two categories:

1. **Deterministic methods.** These are PCA and Isomap. These methods always return the same output no matter how many times they are run on the same input.
2. **Randomized methods.** These are SRP, MDS, t -SNE and UMAP. These methods produce different outputs on multiple runs as they are all initialized with random states.

2.2 Treat Model

Our adversary model is from [BCH22], which is motivated by the treat model in differential privacy [NST⁺21]. We consider an adversary who do not have access to an original training point $x_i \in D$. We assume that this adversary has access to A 's output, as well as all x_j for all $j \neq i$. With this information, their goal is to reconstruct the remaining training points x_i .

Definition 2.1 (Informed adversary). Let M be a dimensionality reduction algorithm, D is a dataset and $\theta = M(D)$. Let x_i be a training point in D . An *informed adversary's* goal is to reconstruct x_i while having access to the following information:

1. M 's output θ ;
2. M 's training algorithm;
3. The *known-member set*: $D_{-i} = D \setminus \{x_i\}$;
4. A public dataset of m data points $D' \in \mathbb{R}^{m \times d}$ that is similar to D .

In particular, the adversary might not have access to the intermediate calculations of M , such as gradients in iterative steps or matrices used in the computation.

While the framework of an informed adversary is unrealistic, it provides a robust framework for demonstrating the feasibility and extent of reconstruction attacks. By assuming an adversary with near-complete knowledge of the dataset, we can rigorously assess the maximum potential for data recovery through such attacks. In addition, this powerful adversarial model offers a stringent test for protective measures. Any defense mechanism capable of withstanding attacks from such a well-informed adversary would, by extension, prove effective against less knowledgeable and more realistic threats.

2.3 Reconstruction Attack

After retrieving θ , D_{-i} and D' in Definition 2.1, the adversary introduces an attack A that outputs a reconstruction \hat{x}_i of x_i . Here, the quality of the reconstruction is measured by a distance function between x_i and \hat{x}_i , which might be task-dependent. In this work, we will only consider the standard Euclidean distance $\|x_i - \hat{x}_i\|$.

The reconstruction attack is related to the attribute inference attack [FLJ⁺14, FJR15, YGFJ18, ZJP⁺20], where some of x_i 's attributes are known to the adversary beforehand, and their goal is to estimate the remaining attributes. Reconstruction attacks can be seen as a generalization of attribute inference attacks, as the former can be used to accomplish the latter, with additional information from the public attributes.

While the original threat model of attribute inference attacks does not necessarily involve an informed adversary, we emphasize that our definition of adversary allows us to quantify the extent of reconstruction given near-complete information of the dataset. Consequently, any successful defense against an informed adversary would also be effective against any attribute inference attack, regardless of the adversary's level of prior knowledge.

3 Our methods

3.1 An overview of the attack

Our reconstruction attack is based on neural network-based attack proposed by [BCH22]. An overview of the attack is displayed in Figure 1.

First, we build a *reconstruction network*, a neural network that takes the low-dimensional embedding θ as input, and then returns a reconstruction \hat{x}_i . The procedure to obtain a reconstruction network (Train-Recon-Net in Algorithm 1) consists of the following steps:

With the known data D_{-i} and public data $D' = \{x'_1, \dots, x'_m\}$. We create a *shadow dataset* that consists of the following inputs and outputs:

- **Input:** $\theta_j = M(z_j)$. Recall that M is the dimensionality reduction model, and $z_j = D_{-i} \cup \{x'_j\}$. Here, $\theta_j \in \mathbb{R}^{2n}$ can be treated as a $2n$ -dimensional input.
- **Output:** x'_j , which is a d -dimensional vector.

As a result, we obtain a dataset $\text{TrainSet} = \{(\theta_1, x'_1), \dots, (\theta_m, x'_m)\}$. We then train a neural network f_{NN} on TrainSet to obtain a reconstruction model. The architecture of f_{NN} will be detailed in the next section.

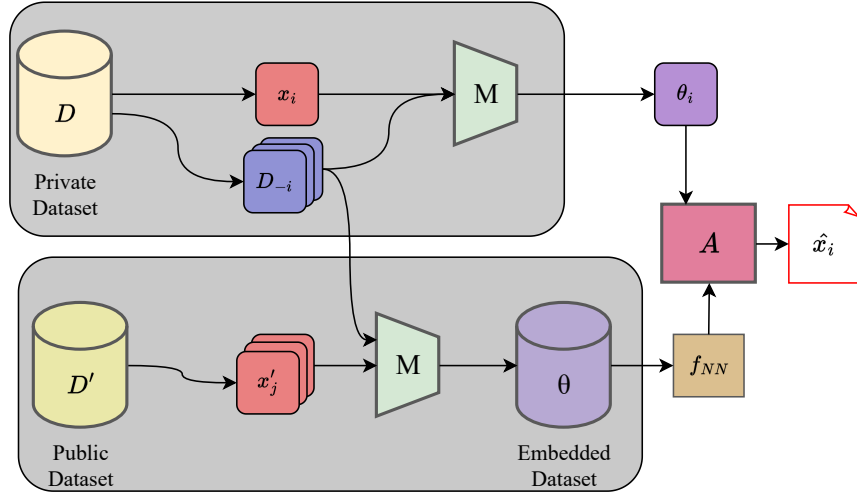


Figure 1: Overview of our reconstruction attack on dimensionality reduction methods.

As $\theta = M(D) = M(D_{-i} \cup \{x_i\})$, we then use the trained network to predict x_i by taking θ as an input. Algorithm 2 details the entire process of the reconstruction attack.

3.2 Reconstruction network

The architecture of f_{NN} follows a standard encoder-decoder design.

The encoder (Table 1) takes an input of size $2n$ and produces an output of a smaller size. In our implementation, we use an output size of 80, though this can be adjusted as needed.

In contrast to previous work, the encoder is specifically designed to reconstruct x_i from a low-dimensional embedding. The $2n$ -dimensional input is first split into two components: the two-dimensional embedding of the target x_i , and the remaining $2n - 2$ dimensions representing the embeddings of other data points. These split inputs are then processed by two separate feedforward layers:

- For the embedding of x_i , a layer with more than two hidden nodes is used in order to expand its representation.
- For the embedding of the other points, a layer with fewer than $2n - 2$ hidden nodes is used in order to compress the contextual information.

The outputs from these two layers are then concatenated to be passed to the decoder.

The decoder receives the encoder’s output and generates a reconstruction matching the size of the original data in the high-dimensional space. Our design follows a standard decoder design for the corresponding output format. Specifically, if the output is one dimensional vector, then the decoder is a standard feedforward neural network. If the output is an image, then the decoder uses the stacked transposed convolutional layers as seen in U-Net-type networks [RFB15]. We will illustrate two examples of the decoders in our experiments on sample datasets.

Algorithm 1 Training reconstruction network

Train-Recon-Net(D_{-i}, D', M, f_{NN})**Input:** Known data points D_{-i} , public data $D' = \{x'_1, \dots, x'_m\}$, target model's algorithm M , reconstruction neural network $f_{NN} : \mathbb{R}^{2n} \rightarrow \mathbb{R}^d$.**Output:** Reconstruction network A .

/* Create shadow training data */

1: Initialize TrainSet = $\{\}$ 2: **for** $j = 1 \dots m$ **do**3: $z_j \leftarrow D_{-i} \cup \{x'_j\}$

▷ Shadow input

4: $\theta_j \leftarrow M(z_j)$

▷ Shadow output

5: TrainSet \leftarrow TrainSet $\cup (z_j, \theta_j)$ 6: **end for**

/* Train reconstruction network */

7: $f \leftarrow$ Train f_{NN} on TrainSet8: **Return:** f

Algorithm 2 Reconstruction attack on dimensionality reduction models

 $A(\theta, D_{-i}, D', M, f_{NN})$ **Input:** Target model's output θ , known data points D_{-i} , public data $D' = \{x'_1, \dots, x'_m\}$, target model's algorithm M , reconstruction neural network $f_{NN} : \mathbb{R}^{2n} \rightarrow \mathbb{R}^d$.**Output:** Reconstruction \hat{x}_i of the i -th data point.1: $f \leftarrow$ Train-Recon-Net(D_{-i}, D', M, f_{NN})2: $\hat{x}_i \leftarrow f(\theta)$ 3: **Return:** \hat{x}_i

3.3 Previous work

Reconstruction attacks based on neural networks were first proposed by [BCH22], who first introduce the notion of an informed adversary (Definition 2.1). In their framework, an adversary with access to a trained machine learning model attempts to reconstruct the model's training data. In particular, the authors propose an attack that uses a neural network, called a *reconstructor network* (RecoNN), that outputs a reconstruction based on the model's parameters. In their work, the reconstruction attack is specifically employed to attack other neural networks. In addition, the authors demonstrate that differential privacy mechanisms can effectively mitigate this type of attack. Related attacks are attribute inference attack [FLJ⁺14, FJR15, YGFJ18, ZJP⁺20], also referred to as model inversion attack [ZJP⁺20]. In these attacks, the adversary knows some of x_i 's features and, with access to the model, attempts to recover the remaining features.

Another well-known attack is the membership inference attack [SSSS17], which aims to determine whether a particular data record was in the model's training set. This attack is performed with black-box queries, meaning that the adversary can only access the model's output on given inputs. To do so, they invented the shadow training technique, which comprises multiple "shadow models" of the target model, each of which is used to simulate members and non-members of the training set that most likely result in the target model's behavior. Then, the attack model is trained on simulated data to classify whether an input is a member or non-member of the training set.

To defend against these attacks, differential privacy [DMNS06, DKM⁺06] is considered a powerful

| Layer | Parameters | | |
|--------------------------------|------------|---|----------|
| Input | $2n$ | | |
| Split | 2 | + | $2n - 2$ |
| Fully connected ($\times 2$) | 16 | + | 64 |
| Concatenate | 80 | | |

Table 1: Encoder of the reconstruction network.

privacy-preserving framework. A dataset query is differentially private if an adversary, even with knowledge of all but one data points, could hardly learn anything about the remaining data point from the query’s output. In the context of dimensionality reduction, research has shown that the random projection can achieve differential privacy [BBDS12, KKMM13]. And a differentially private algorithm that approximates PCA was first proposed by [BDMN05], followed by a long line of research to improve the output quality, with notable contributions from [CSS13, HR13, DTTZ14, HP14] and [LKJO22]. Nonetheless, differential privacy analyses of other dimensionality reduction methods remain scarce, largely due to the complex nature of their outputs.

How is attack on dimensionality reduction model different from previous work? Previous work on neural network-based reconstruction attacks have mainly focused on supervised learning models, using model parameters as input for reconstruction. Our method, in contrast, takes embedded data in low-dimensional space as input. This distinction results in the following key differences:

1. **Input dimension.** Our reconstruction network takes low-dimensional embedded data as input with a dimension of $2n$. This is often smaller than the number of parameters in large neural networks.
2. **Direct information extraction.** Dimensionality reduction models preserve a direct correspondence between input and output data. Specifically, the information of an input point x_i is directly contained in the i -th row of the output. And the data points that are close to x_i in the low-dimensional space are likely to be close to x_i in the high-dimensional space as well. As a consequence, an informed adversary can gain significant information about x_i with a complete knowledge of the remaining $n - 1$ points. This is in contrast to supervised learning models, where individual data point information cannot be directly extracted from the model parameters. This observation motivates the modular design of the encoder in Table 1.

4 Experiments

4.1 MNIST dataset

The MNIST dataset consists of grayscale images of handwritten digits ranging from 0 to 9. Their dimensions are 28×28 . The dataset has 60,000 images for training and 10,000 for testing. They are commonly used for training machine and deep learning models for classification and image processing tasks.

Due to computational constraint, we took a random subset of 5,000 images from the training set and divided them into three parts (1) a training set with 4,000 samples, (2) a validation set with

| Layer | Parameters |
|---|--|
| Tranposed convolution + Batchnorm + ReLU | 512 filters of 4×4 , strides 1, padding 0 |
| Tranposed convolution + Batchnorm + ReLU | 256 filters of 4×4 , stride 2, padding 1 |
| Tranposed convolution + Batchnorm + ReLU | 128 filters of 4×4 , strides 2, padding 1 |
| Tranposed convolution + Batchnorm + ReLU | 64 filters of 4×4 , strides 2, padding 1 |
| Tranposed Convolution ReLU | 1 filters of 1×1 , strides 1, padding 2 28 \times 28 units |

Table 2: Decoder of the reconstruction network for the MNIST dataset.

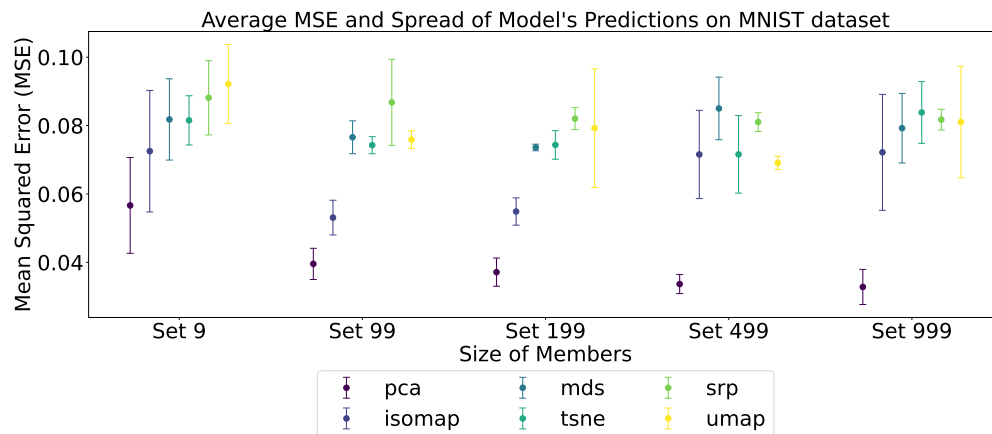


Figure 2: Average MSE with one standard deviation of the reconstructions on six dimensionality reduction models trained on the MNIST dataset, with the number of the known members ranging from 9 to 999.

500 samples, and (3) a test set with 500 samples. From the remaining images, we randomly selected a set of $S \in \{9, 99, 199, 499, 999\}$ images to form the known-member set D_{-i} (see Definition 2.1).

We prepared shadow datasets for the reconstruction network following the Step 1 – 6 outlined in Algorithm 1. Specifically, we applied each of the six dimensionality reduction methods (PCA, SRP, MDS, Isomap, t-SNE, and UMAP) to $x \cup D_{-i}$ for each x in the training, validation, and test set. As a result, we obtained shadow training, validation, and test sets for the reconstruction network with the embedding as the input and the original image x as the output.

In the training stage, The shadow training set were split into minibatches, each with size of 64. The architectures of the reconstruction network’s encoder and decoder are described in Table 1 and 2, respectively. In particular, as the output of the network is a 2D image, the decoder consists of multiple transposed convolutional layers. We also applied batch normalization, and ReLU as the activation function. Our loss function is a combined MSE loss and L1 loss, with Adam [KB15] as the optimizer. Moreover, even though we defined the epoch at 500 and the learning rate at 1×10^{-5} , early stopping was very essential because it can prevent models from overfitting.

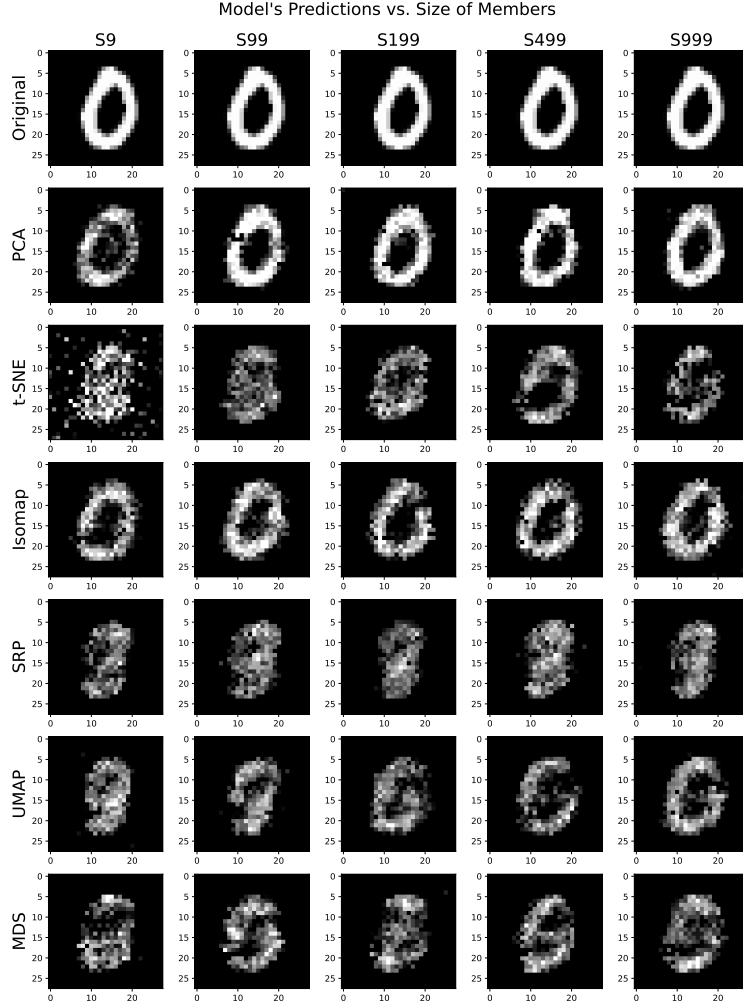


Figure 3: Examples of outputs from reconstruction attacks on six dimensionality reduction models trained on the MNIST dataset, with the number of known members varying from 9 to 999.

The data preparation and training procedure were repeated for every dimensionality reduction methods and every known-member set size $S \in \{9, 99, 199, 499, 999\}$. In addition, to account for variation in the known-member sets, we repeated each combination five times. We then reported the average and the standard deviation of the mean squared error (MSE) on the shadow test set.

Figure 2 presents the reconstruction MSEs for the six dimensionality reduction methods across the five known-member set sizes. The results reveal that PCA is the most vulnerable method, indicated by its comparatively small MSEs. Moreover, PCA's MSE shows a declining trend as the known-member set size increases, indicating that the quality of reconstructions improves when the adversary has access to more data points.

For the other models, attacks on Isomap perform well on small known-member set sizes. However, as the set size increases to 499 or 999, attacks on the Isomap and the other models besides PCA becomes more difficult as indicated by their relatively large MSEs. By comparing the averages, we notice that MDS is consistently the third most vulnerable model, while SRP is the least vulnerable

| Layer | Parameters |
|---|--|
| Tranposed convolution + Batchnorm + ReLU | 512 filters of 4×4 , strides 1, padding 0 |
| Tranposed convolution + Batchnorm + ReLU + Dropout | 1024 filters of 4×4 , stride 2, padding 1 |
| Tranposed convolution + Batchnorm + ReLU | 512 filters of 4×4 , strides 2, padding 1 |
| Tranposed convolution + Batchnorm + ReLU | 256 filters of 4×4 , strides 2, padding 1 |
| Tranposed Convolution ReLU | 1 filters of 4×4 , strides 2, padding 1 64×64 units |

Table 3: Decoder of the reconstruction network for the NIH Chest X-ray dataset.

model across all set sizes.

Examples of an image reconstructions are displayed in Figure 3. We can see that the reconstructions from attacks on PCA and Isomap closely resemble the original image, aligning with the lower MSE values discussed earlier. For the other methods, attacks on t -SNE, MDS, and UMAP show moderate success when the known-member set size is 499 or 999. In contrast, attacks on SRP is the least successful among all methods tested, as their reconstructions barely resemble the original image.

4.2 NIH Chest X-ray dataset

For our second experiment, we considered a more complex dataset. We considered the NIH Chest X-ray dataset [WPL⁺17], which consists of 112,120 frontal-view X-ray images of 30,805 unique patients. We first reduced the image size from 1024×1024 to 64×64 . We randomly selected a subset of 5,000 images from the dataset, which was then separated into 4,000 images for training, 500 images for validation, and 500 images for testing.

Following the same data preparation procedure for MNIST, we constructed shadow training, validation, and test sets from the original dataset. We changed our model’s architecture a little bit to fit the size of an output image (as detailed in Table 3). However, all hyperparameters were still the same as MNIST.

We repeated the data preparation and model training five times to account for the variation in the known-member sets. Figure 4 presents the average MSE along with one standard deviation for each method and each known-member set size. Consistent with our findings from the MNIST dataset, these results indicate that PCA remains the most vulnerable dimensionality reduction model. However, unlike the MNIST results, we observe no clear declining trend in the average MSE as the known-member set size increases. In addition, Isomap is the second most vulnerable method (except at $S = 499$), and SRP is the least vulnerable method.

Figure 5 displays examples of X-ray image reconstructions from our attacks. Unlike the MNIST results, these reconstructions show notably poorer quality across all methods and known-member set sizes, though they still bear some resemblance to the original images. Nonetheless, we can still notice differences in the reconstruction quality among the methods. Attacks on PCA consistently produce the best reconstructions, as indicated by darker chest areas and the absence of artifacts. In

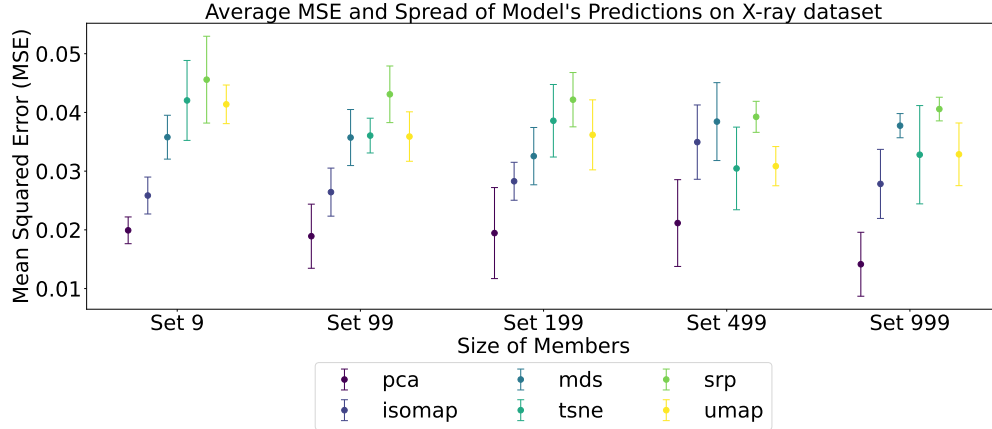


Figure 4: Average MSE with one standard deviation of the reconstructions on six dimensionality reduction models trained on the NIH Chest X-ray dataset, with the number of the known members ranging from 9 to 999.

contrast, attacks on SRP is the least successful, as they produce the fuzziest images compared to the other methods.

5 Discussion

We summarize our findings from these two experiments:

- The attack is most effective against PCA and least effective against SRP across both datasets, as demonstrated both quantitatively by the MSE plots and qualitatively through the reconstruction examples.
- The attack is effective on non-randomized algorithms and ineffective on randomized algorithms.

The deterministic methods (PCA and Isomap) not only produce the same results when applied on the same dataset, but also show only slight changes in output when a single data point is modified. As a result, it is relatively easy for the reconstruction network to identify patterns in the low-dimensional representations and accurately recreate the original high-dimensional data.

The randomized methods (SRP, MDS, *t*-SNE and UMAP), on the other hand, start with random initializations that can end up with totally different outputs in different runs, even when fitting on the same dataset. This results in diverse patterns in the shadow dataset that are particularly difficult for our reconstruction network to learn.

Our results indicate that when data privacy is a primary concern in the publication of low-dimensional embeddings, randomized algorithms are preferable, as their inherent variability makes them more resistant to the reconstruction attack.

- Our results show the most significant improvement when increasing the size of the known-member set from $S = 9$ to $S = 99$. However, for some models, further increases in S lead to

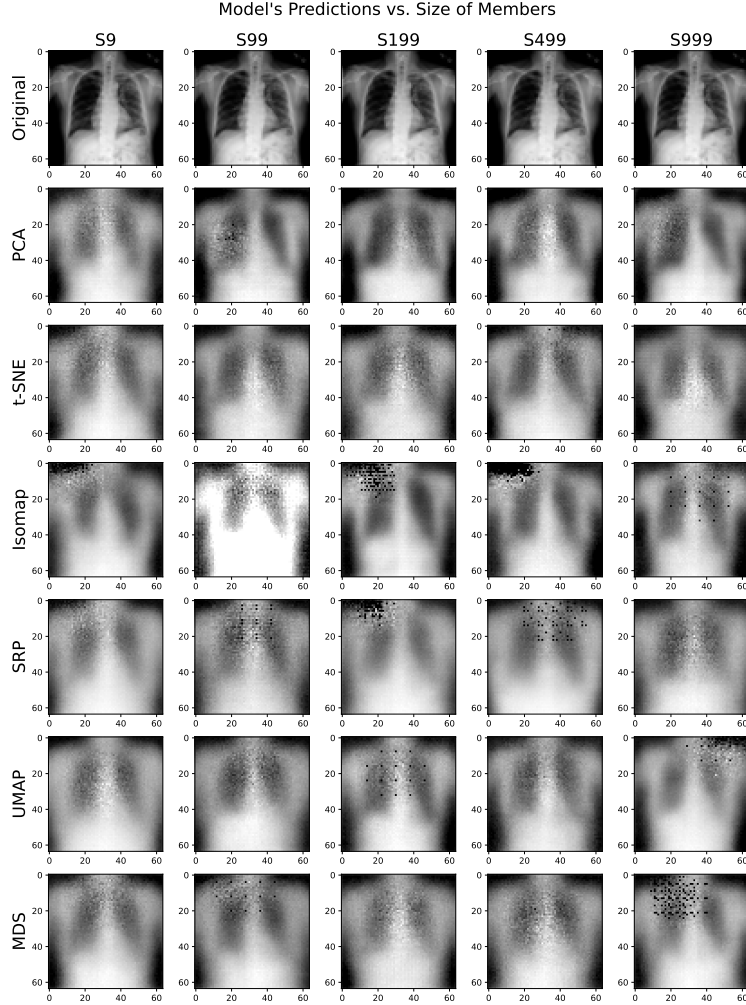


Figure 5: Examples of outputs from reconstruction attacks on six dimensionality reduction models trained on the NIH Chest X-ray dataset, with the number of known members varying from 9 to 999.

decreased attack performance. This counterintuitive effect occurs because the input dimension of the reconstruction network ($2n$) grows with S (where $S = n - 1$). As the input dimension increases, the network requires more complexity and a larger number of shadow training samples to effectively learn from such high-dimensional data.

This observation suggests that the attack can potentially become stronger as S increases, but this can only be achieved with a larger public dataset, a more complex network architecture and more computation resources.

6 Defense against the reconstruction attack

To defend against reconstruction attacks, we investigate an additive noise mechanism. This approach involves adding independent noise, sampled from a normal distribution, to the high-dimensional

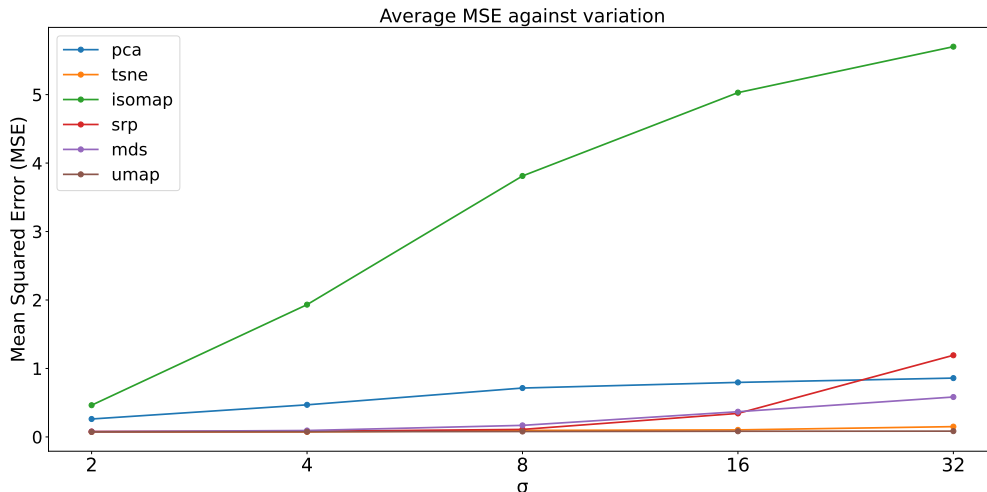


Figure 6: Average MSE on each scale of noises for every dimensionality reduction methods.

data prior to dimensionality reduction. To assess how the scale of noise affects reconstruction quality, we apply this technique to the MNIST dataset. Specifically, we add normally distributed noise to each image x as follows:

$$x + \varepsilon, \quad \varepsilon \sim \mathcal{N}(\mathbf{0}, \sigma^2 I_d).$$

where d is the dimension of x and $\sigma \in \{2, 4, 8, 16, 32\}$. We feed noisy images into various dimensionality reduction methods, whose outputs are then passed on to our reconstruction networks that were trained on non-noisy data. Figure 6 illustrates the MSEs of the reconstruction with $S = 99$ for each dimensionality reduction model. The results demonstrate that the additive noise mechanism is highly effective for certain reduction methods. Notably, Isomap appears to be the most significantly affected by the added noise, as indicated by relatively large MSEs compared to other models.

Figure 7 provides examples of reconstructions from noisy images. Interestingly, while only Isomap shows high MSE values, both PCA and Isomap reconstructions become fully distorted at high noise levels, suggesting that privacy is preserved in these two models' outputs after adding noises to the original image. In particular, the reconstruction of Isomap at high noise levels consists mostly of high pixel values, which is consistent with the high MSEs in Figure 6. We also observe that the reconstructions for the randomized methods somewhat resemble a digit even with a high level of noises, indicating that the reconstruction networks have learned sufficiently diverse outputs from these methods that it is able to output digit-like images even from noisy lower-dimensional embeddings.

7 Conclusion

Dimensionality reduction methods can help improve data interpretation and reduce model training costs. However, while these methods do not directly reveal the original data, they may inadvertently leak sensitive information. In this study, we propose a reconstruction attack in the context of an informed adversary to assess how much individual information is leaked from the published outputs of various dimensionality reduction methods.

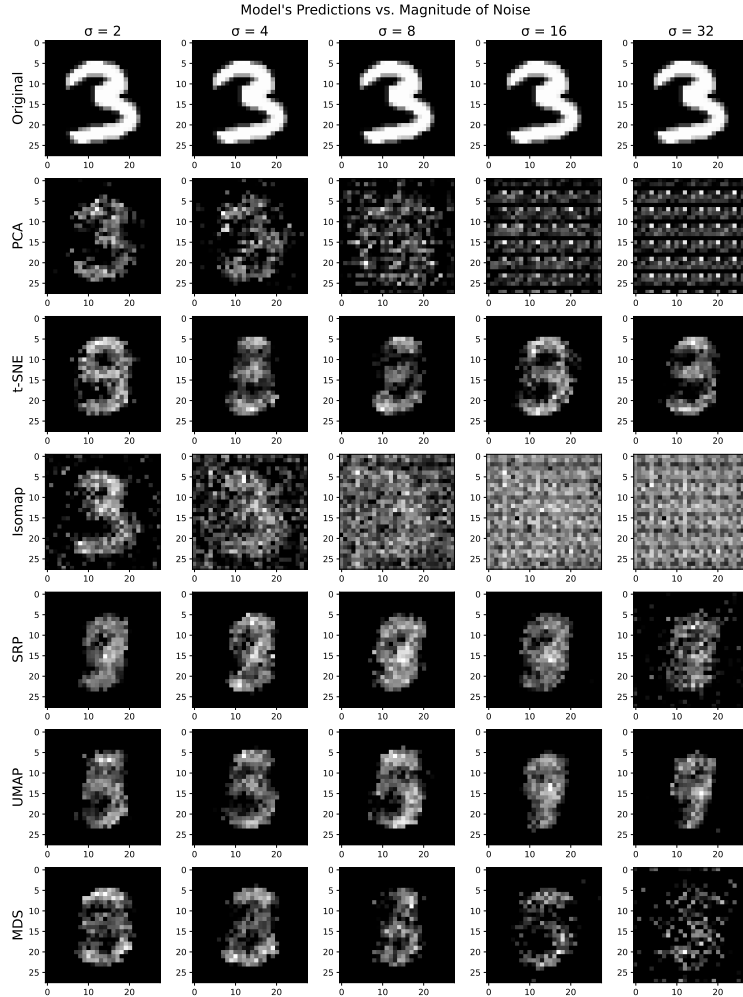


Figure 7: Outputs of reconstruction attack on embeddings of a noisy image in MNIST.

We propose to use a neural network to reconstruct the original data. Our proposed network is specifically designed to exploit the order-preservation nature of the dimensionality reduction models and separate the low-dimensional embedding of an individual from the rest. In our experiments, we perform the reconstruction attack on six dimensionality reduction models on the MNIST and NIH Chest X-ray datasets. The results empirically indicate that the reconstruction attack is relatively effective on the deterministic algorithms, namely PCA and Isomap. In contrast, methods that utilize random initialization, namely SRP, MDS, t-SNE, and UMAP, show greater resilience to these attacks. In particular, based on both quantitative metrics and qualitative analysis, SRP demonstrates the highest resilience among the evaluated models. We also find that The attack’s effectiveness increases with the adversary’s knowledge of data points. However, this improvement comes at a cost, as it requires a larger public dataset, a more complex model architecture, and more computational resources.

We also suggest an additive noise mechanism to defend against the reconstruction attack. Our experiment shows that the reconstructions for PCA and Isomap becomes highly distorted at high

noise levels. This implies that the mechanism is effective for these two methods. The mechanism is also effective on the randomized methods, but the reconstructions are not completely distorted but still somewhat resemble sample points in the high-dimensional data space.

References

- [Ach01] Dimitris Achlioptas. Database-friendly random projections. In *Proceedings of the twentieth ACM SIGMOD-SIGACT-SIGART symposium on Principles of database systems*, SIGMOD/PODS01. ACM, May 2001.
- [BBDS12] Jeremiah Blocki, Avrim Blum, Anupam Datta, and Or Sheffet. The johnson-lindenstrauss transform itself preserves differential privacy. In *2012 IEEE 53rd Annual Symposium on Foundations of Computer Science*, pages 410–419, 2012.
- [BCH22] Borja Balle, Giovanni Cherubin, and Jamie Hayes. Reconstructing training data with informed adversaries. In *2022 IEEE Symposium on Security and Privacy (SP)*. IEEE, May 2022.
- [BDMN05] Avrim Blum, Cynthia Dwork, Frank McSherry, and Kobbi Nissim. Practical privacy: the sulq framework. In *Proceedings of the twenty-fourth ACM SIGMOD-SIGACT-SIGART symposium on Principles of database systems*, SIGMOD/PODS05. ACM, June 2005.
- [CCR⁺20] Matthew C. Cieslak, Ann M. Castelfranco, Vittoria Roncalli, Petra H. Lenz, and Daniel K. Hartline. t-distributed stochastic neighbor embedding (t-sne): A tool for eco-physiological transcriptomic analysis. *Marine Genomics*, 51:100723, 2020.
- [CLE⁺19] Nicholas Carlini, Chang Liu, Úlfar Erlingsson, Jernej Kos, and Dawn Song. The secret sharer: Evaluating and testing unintended memorization in neural networks. In *28th USENIX Security Symposium (USENIX Security 19)*, pages 267–284, Santa Clara, CA, August 2019. USENIX Association.
- [CSS13] Kamalika Chaudhuri, Anand D. Sarwate, and Kaushik Sinha. A near-optimal algorithm for differentially-private principal components. *Journal of Machine Learning Research*, 14(89):2905–2943, 2013.
- [CTW⁺21] Nicholas Carlini, Florian Tramèr, Eric Wallace, Matthew Jagielski, Ariel Herbert-Voss, Katherine Lee, Adam Roberts, Tom Brown, Dawn Song, Úlfar Erlingsson, Alina Oprea, and Colin Raffel. Extracting training data from large language models. In *30th USENIX Security Symposium (USENIX Security 21)*, pages 2633–2650. USENIX Association, August 2021.
- [DKM⁺06] Cynthia Dwork, Krishnaram Kenthapadi, Frank McSherry, Ilya Mironov, and Moni Naor. Our data, ourselves: Privacy via distributed noise generation. In *Advances in Cryptology - EUROCRYPT 2006, 25th Annual International Conference on the Theory and Applications of Cryptographic Techniques*, volume 4004 of *Lecture Notes in Computer Science*, pages 486–503. Springer, 2006.

- [DMNS06] Cynthia Dwork, Frank McSherry, Kobbi Nissim, and Adam Smith. Calibrating noise to sensitivity in private data analysis. In Shai Halevi and Tal Rabin, editors, *Theory of Cryptography*, pages 265–284, Berlin, Heidelberg, 2006. Springer Berlin Heidelberg.
- [DSK⁺23] Anant Dadu, Vipul K. Satone, Rachneet Kaur, Mathew J. Koretsky, Hirotaka Iwaki, Yue A. Qi, Daniel M. Ramos, Brian Avants, Jacob Hesterman, Roger Gunn, Mark R. Cookson, Michael E. Ward, Andrew B. Singleton, Roy H. Campbell, Mike A. Nalls, and Faraz Faghri. Application of aligned-umap to longitudinal biomedical studies. *Patterns*, 4(6):100741, June 2023.
- [DTTZ14] Cynthia Dwork, Kunal Talwar, Abhradeep Thakurta, and Li Zhang. Analyze gauss: optimal bounds for privacy-preserving principal component analysis. In *Proceedings of the forty-sixth annual ACM symposium on Theory of computing*, STOC '14. ACM, May 2014.
- [FJR15] Matt Fredrikson, Somesh Jha, and Thomas Ristenpart. Model inversion attacks that exploit confidence information and basic countermeasures. In *Proceedings of the 22nd ACM SIGSAC Conference on Computer and Communications Security*, CCS'15. ACM, October 2015.
- [FLJ⁺14] Matthew Fredrikson, Eric Lantz, Somesh Jha, Simon Lin, David Page, and Thomas Ristenpart. Privacy in pharmacogenetics: An End-to-End case study of personalized warfarin dosing. In *23rd USENIX Security Symposium (USENIX Security 14)*, pages 17–32, San Diego, CA, August 2014. USENIX Association.
- [Hot33] H. Hotelling. Analysis of a complex of statistical variables into principal components. *Journal of Educational Psychology*, 24(6):417–441, September 1933.
- [HP14] Moritz Hardt and Eric Price. The noisy power method: A meta algorithm with applications. In Z. Ghahramani, M. Welling, C. Cortes, N. Lawrence, and K.Q. Weinberger, editors, *Advances in Neural Information Processing Systems*, volume 27. Curran Associates, Inc., December 2014.
- [HR13] Moritz Hardt and Aaron Roth. Beyond worst-case analysis in private singular vector computation. In *Proceedings of the forty-fifth annual ACM symposium on Theory of Computing*, STOC'13. ACM, June 2013.
- [JL84] William B. Johnson and Joram Lindenstrauss. Extensions of lipschitz mappings into a hilbert space. *Conference on Modern Analysis and Probability*, page 189–206, 1984.
- [KB15] Diederik P. Kingma and Jimmy Ba. Adam: A method for stochastic optimization. In Yoshua Bengio and Yann LeCun, editors, *3rd International Conference on Learning Representations, ICLR 2015, San Diego, CA, USA, May 7-9, 2015, Conference Track Proceedings*, 2015.
- [KB19] Dmitry Kobak and Philipp Berens. The art of using t-sne for single-cell transcriptomics. *Nature Communications*, 10(1), November 2019.

- [KKMM13] Krishnaram Kenthapadi, Aleksandra Korolova, Ilya Mironov, and Nina Mishra. Privacy via the johnson-lindenstrauss transform. *Journal of Privacy and Confidentiality*, 5(1), August 2013.
- [Kru64] J. B. Kruskal. Multidimensional scaling by optimizing goodness of fit to a nonmetric hypothesis. *Psychometrika*, 29(1):1–27, March 1964.
- [LHC06] Ping Li, Trevor J. Hastie, and Kenneth W. Church. Very sparse random projections. In *Proceedings of the 12th ACM SIGKDD international conference on Knowledge discovery and data mining*, KDD06. ACM, August 2006.
- [LKJO22] Xiyang Liu, Weihao Kong, Prateek Jain, and Sewoong Oh. Dp-pca: Statistically optimal and differentially private pca. In S. Koyejo, S. Mohamed, A. Agarwal, D. Belgrave, K. Cho, and A. Oh, editors, *Advances in Neural Information Processing Systems*, volume 35, pages 29929–29943. Curran Associates, Inc., 2022.
- [LX20] Yongjing Lin and Huosheng Xie. Face gender recognition based on face recognition feature vectors. In *2020 IEEE 3rd International Conference on Information Systems and Computer Aided Education (ICISCAE)*, pages 162–166, 2020.
- [MHM18] Leland McInnes, John Healy, and James Melville. Umap: Uniform manifold approximation and projection for dimension reduction, 2018.
- [NBA⁺21] Salifu Nanga, Ahmed Tijani Bawah, Benjamin Ansah Acquaye, Mac-Issaka Billa, Francis Delali Baeta, Nii Afotey Odai, Samuel Kwaku Obeng, and Ampem Darko Nsiah. Review of dimension reduction methods. *Journal of Data Analysis and Information Processing*, 09(03):189–231, 2021.
- [NST⁺21] Milad Nasr, Shuang Songi, Abhradeep Thakurta, Nicolas Papernot, and Nicholas Carlin. Adversary instantiation: Lower bounds for differentially private machine learning. In *2021 IEEE Symposium on Security and Privacy (SP)*. IEEE, May 2021.
- [Pea01] Karl Pearson. Liii. on lines and planes of closest fit to systems of points in space. *The London, Edinburgh, and Dublin Philosophical Magazine and Journal of Science*, 2(11):559–572, 1901.
- [Pla13] Alexander Platzer. Visualization of snps with t-sne. *PLoS ONE*, 8(2):e56883, February 2013.
- [RFB15] Olaf Ronneberger, Philipp Fischer, and Thomas Brox. *U-Net: Convolutional Networks for Biomedical Image Segmentation*, page 234–241. Springer International Publishing, 2015.
- [SSSS17] Reza Shokri, Marco Stronati, Congzheng Song, and Vitaly Shmatikov. Membership inference attacks against machine learning models. In *2017 IEEE Symposium on Security and Privacy (SP)*. IEEE, May 2017.
- [TEAYT⁺19] Shadi Toghi Eshghi, Amelia Au-Yeung, Chikara Takahashi, Christopher R. Bolen, Maclean N. Nyachienga, Sean P. Lear, Cherie Green, W. Rodney Mathews, and William E. O’Gorman. Quantitative comparison of conventional and t-sne-guided gating analyses. *Frontiers in Immunology*, 10, 2019.

- [TSL00] Joshua B. Tenenbaum, Vin de Silva, and John C. Langford. A global geometric framework for nonlinear dimensionality reduction. *Science*, 290(5500):2319–2323, December 2000.
- [vdMH08] Laurens van der Maaten and Geoffrey Hinton. Visualizing data using t-sne. *Journal of Machine Learning Research*, 9(86):2579–2605, 2008.
- [WPL⁺17] Xiaosong Wang, Yifan Peng, Le Lu, Zhiyong Lu, Mohammadhadi Bagheri, and Ronald M. Summers. Chestx-ray8: Hospital-scale chest x-ray database and benchmarks on weakly-supervised classification and localization of common thorax diseases. In *Proceedings of the IEEE Conference on Computer Vision and Pattern Recognition (CVPR)*, July 2017.
- [XZS⁺22] Jiazhi Xia, Yuchen Zhang, Jie Song, Yang Chen, Yunhai Wang, and Shixia Liu. Revisiting dimensionality reduction techniques for visual cluster analysis: An empirical study. *IEEE Transactions on Visualization and Computer Graphics*, 28(1):529–539, 2022.
- [YGFJ18] S. Yeom, I. Giacomelli, M. Fredrikson, and S. Jha. Privacy risk in machine learning: Analyzing the connection to overfitting. In *2018 IEEE 31st Computer Security Foundations Symposium (CSF)*, pages 268–282, Los Alamitos, CA, USA, jul 2018. IEEE Computer Society.
- [ZJP⁺20] Y. Zhang, R. Jia, H. Pei, W. Wang, B. Li, and D. Song. The secret revealer: Generative model-inversion attacks against deep neural networks. In *2020 IEEE/CVF Conference on Computer Vision and Pattern Recognition (CVPR)*, pages 250–258, Los Alamitos, CA, USA, jun 2020. IEEE Computer Society.